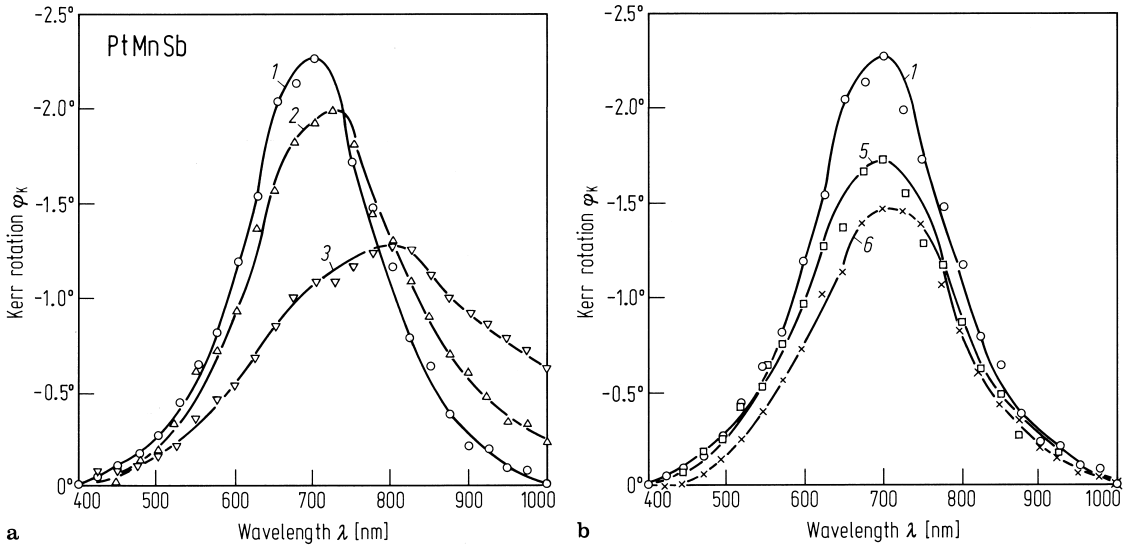

Fig. 610. Spectra of the Kerr rotation angle φ_K for samples in the PtMnSb ternary system: the number of the samples and their composition are given in Table 130 [90T2].

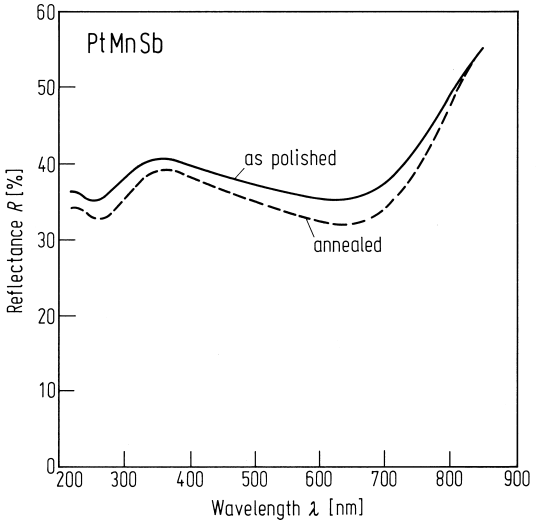

Fig. 611. Spectra of reflectance R for PtMnSb, as polished and annealed at 500 °C for 2 hours [88T2].

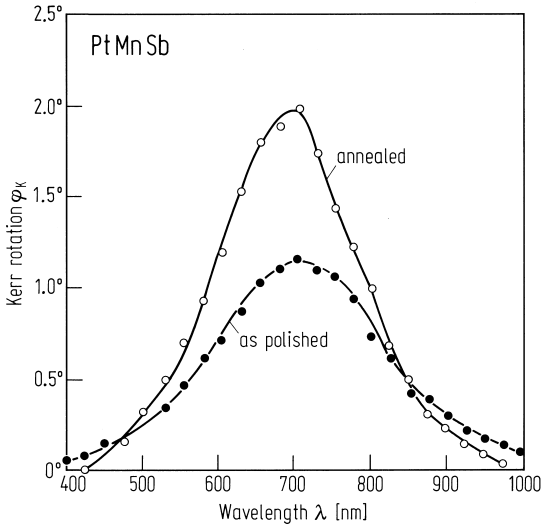

Fig. 612. Spectra of the polar Kerr rotation angle φ_K for PtMnSb as polished and annealed at 500 °C for 2 hours [88T2].

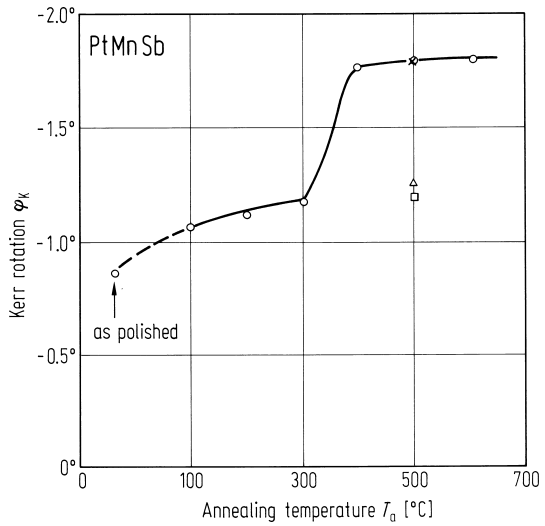

Fig. 613. Annealing temperature dependence of the polar Kerr rotation angle φ_K for PtMnSb in the case of the annealing time of 2 hours. Triangle and cross show the values for thin films annealed at 500 °C reported in [87O1] and [87I2]. Results of [88T2] are indicated by a square [88T2].

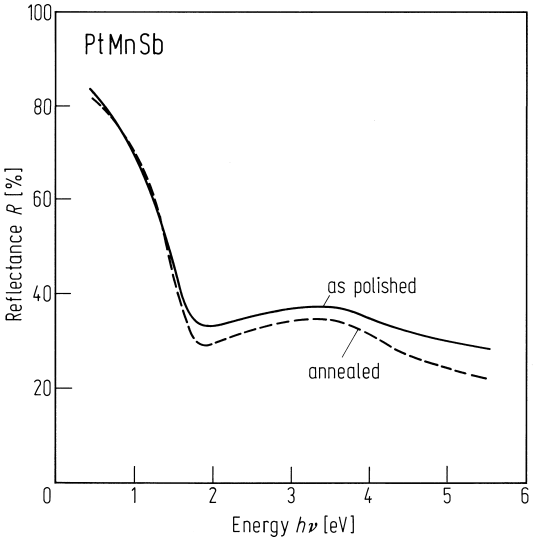

Fig. 616. Spectra of the reflectance R for $Pt_{1.00}Mn_{1.00}Sb_{1.00}$: as polished and annealed at 500 °C after polishing [91T1].

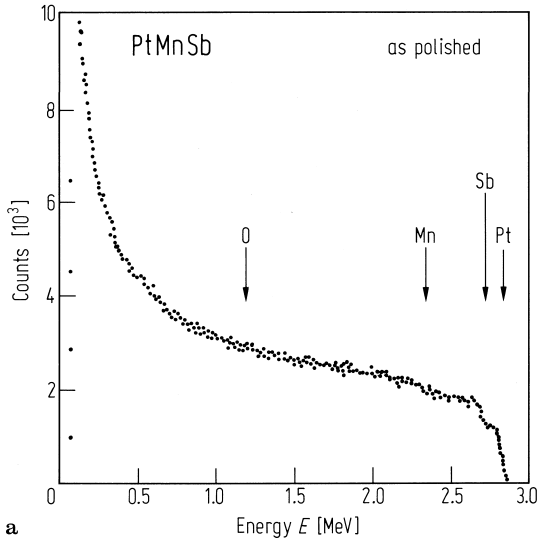

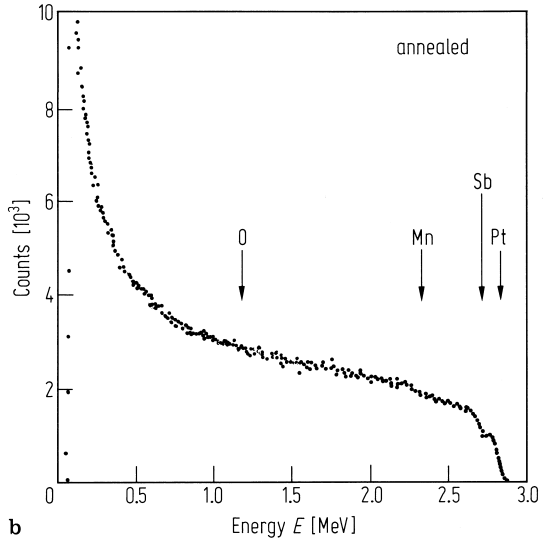

Fig. 614. The Rutherford backscattering spectra (RBS) spectra for the surfaces of PtMnSb (**a**) as polished and (**b**) annealed at 500 °C for 2 hours. The arrows indicate the energies corresponding to the respective elements if they are at the top surface [88T2].

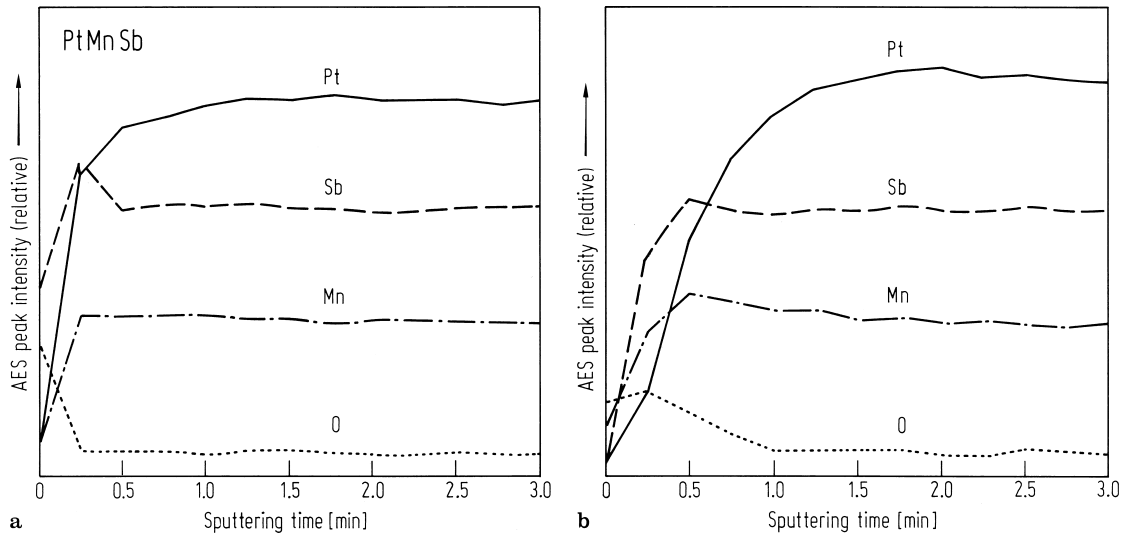

Fig. 615. The AES depth profiles of Pt, Mn, Sb and O atoms at the surfaces of PtMnSb (**a**) as polished and (**b**) annealed at 500 °C for 2 hours [88T2].

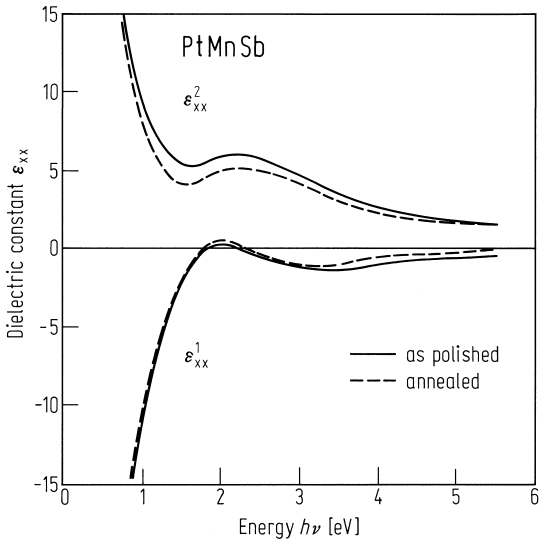

Fig. 617. Spectra of the real (ε^1_{xx}) and imaginary (ε^2_{xx}) parts of diagonal dielectric constants for $Pt_{1.00}Mn_{1.00}Sb_{1.00}$: as polished and annealed at 500 °C after polishing [91T1].

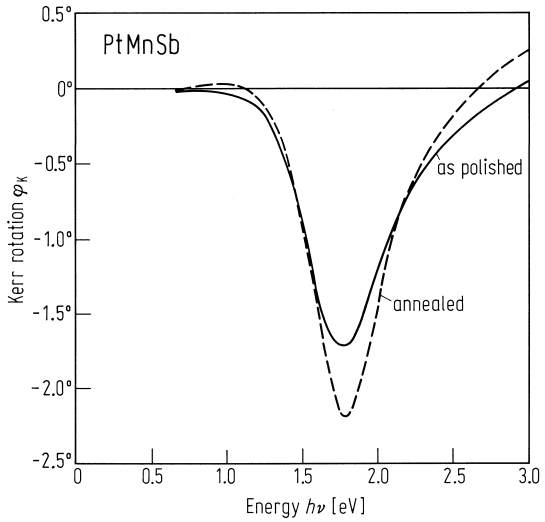

Fig. 618. Spectra of the Kerr rotation φ_K for PtMnSb: as polished and annealed at 500 °C after polishing [91T1].

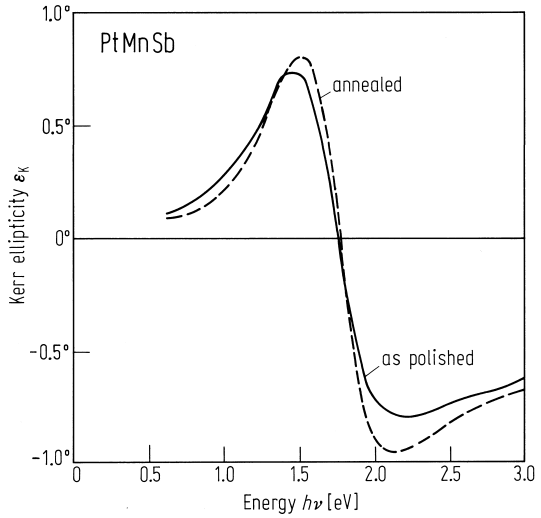

Fig. 619. Spectra of the Kerr ellipticity ε_K for PtMnSb: as polished and annealed at 500 °C after polishing [91T1].

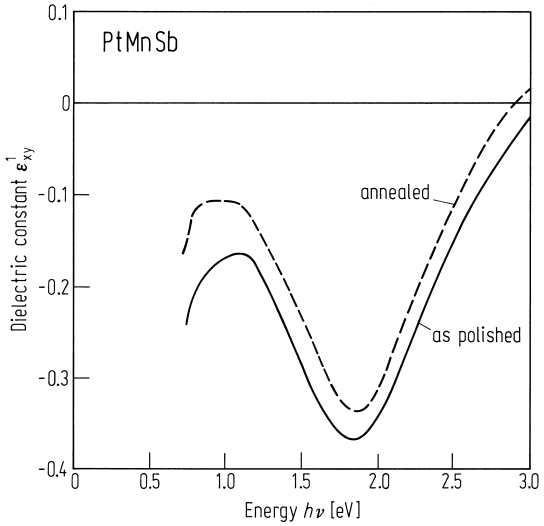

Fig. 620. Spectra of the real part (ε^1_{xy}) of the off-diagonal dielectric constants for PtMnSb: as polished and annealed at 500 °C after polishing [91T1].

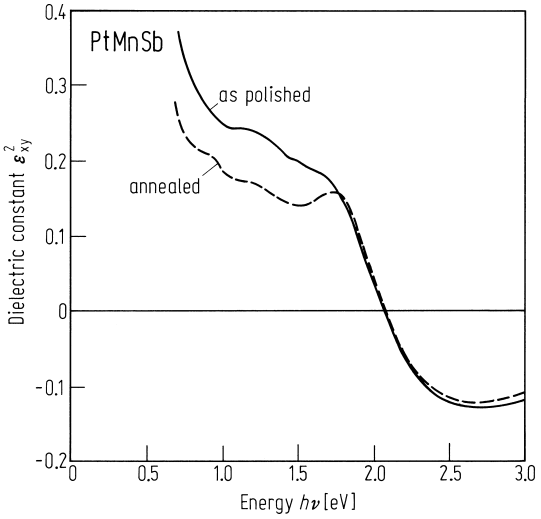

Fig. 621. Spectra of the imaginary part (ε^2_{xy}) of the off-diagonal dielectric constants for PtMnSb: as polished and annealed at 500 °C after polishing [91T1].

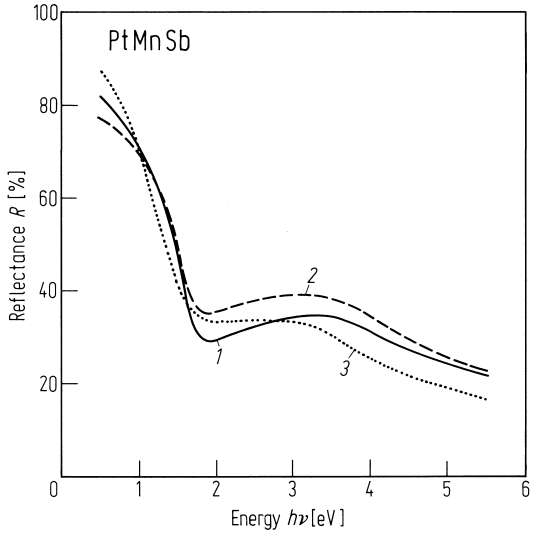

Fig. 622. Spectra of the reflectance R for $Pt_{1.00}Mn_{1.00}Sb_{1.00}$ (*1*), $Pt_{1.05}Mn_{0.90}Sb_{1.05}$ (*2*) and $Pt_{0.95}Mn_{1.10}Sb_{0.95}$ (*3*) [91T1].

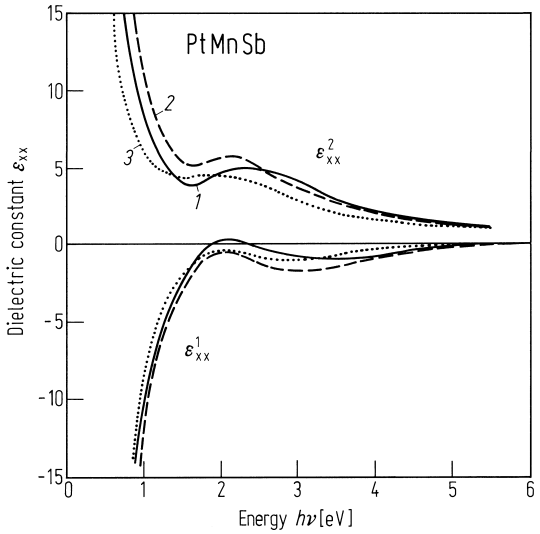

Fig. 623. Spectra of the real (ε^1_{xx}) and imaginary (ε^2_{xx}) parts of the diagonal dielectric constants for $Pt_{1.00}Mn_{1.00}Sb_{1.00}$, (*1*), $Pt_{1.05}Mn_{0.90}Sb_{1.05}$ (*2*) and $Pt_{0.95}Mn_{1.10}Sb_{0.95}$ (*3*) [91T1].

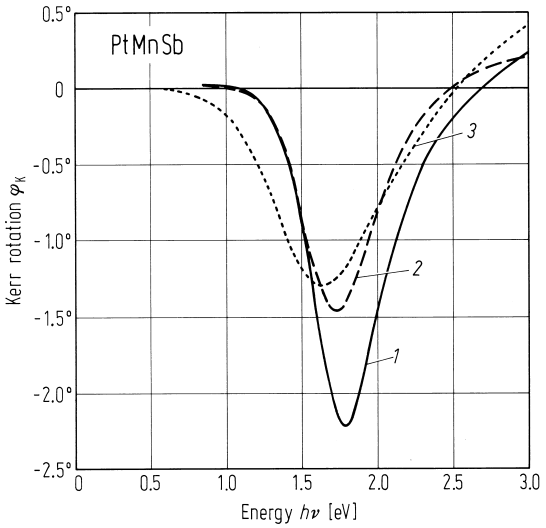

Fig. 624. Spectra of the Kerr rotation φ_K for PtMnSb (*1*), $Pt_{1.05}$ $Mn_{0.90}Sb_{1.05}$ (*2*) and $Pt_{0.95}$,$Mn_{1.10}Sb_{0;95}$ (*3*) [91T1].

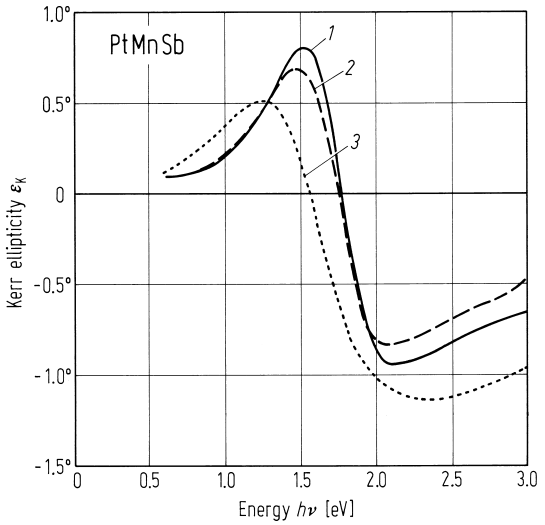

Fig. 625. Spectra of the Kerr ellipticity ε_K for PtMnSb (*1*), $Pt_{1.05}$ $Mn_{0.90}Sb_{1.05}$ (*2*) and $Pt_{0.95}$,$Mn_{1.10}Sb_{0;95}$ (*3*) [91T1].

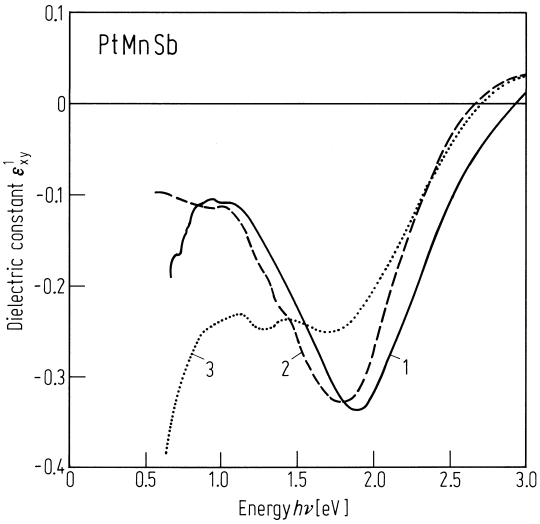

Fig. 626. Spectra of the real part (ε^1_{xy}) of the off-diagonal dielectric constant for PtMnSb (*1*), $Pt_{1.05}Mn_{0.9}Sb_{1.05}$ (*2*) and $Pt_{0.95}Mn_{1.10}Sb_{0.95}$ (*3*) [91T1].

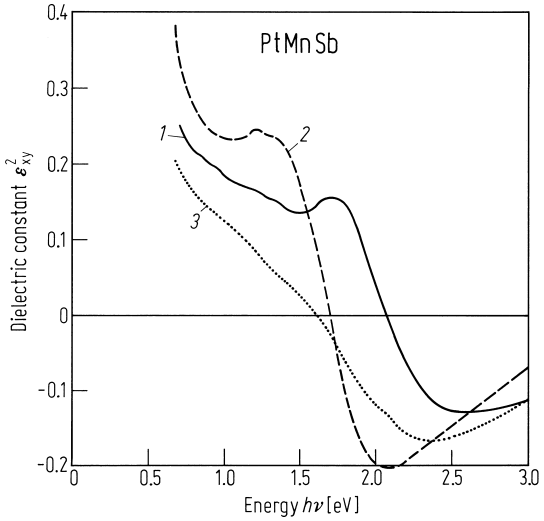

Fig. 627. Spectra of the imaginary part ε^2_{xy} of off-diagonal dielectric constants for PtMnSb (*1*), $Pt_{1.05}Mn_{0.90}Sb_{1.05}$ (*2*) and $Pt_{0.95}Mn_{1.10}Sb_{0.95}$ (*3*) [91T1].

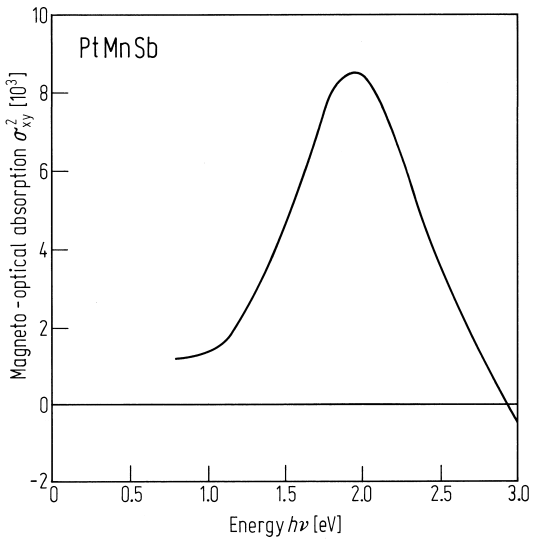

Fig. 628. Spectra of the magneto-optical absorption σ^2_{xy} for $Pt_{1.00}Mn_{1.00}Sb_{1.00}$ in the annealed state. [91T1].

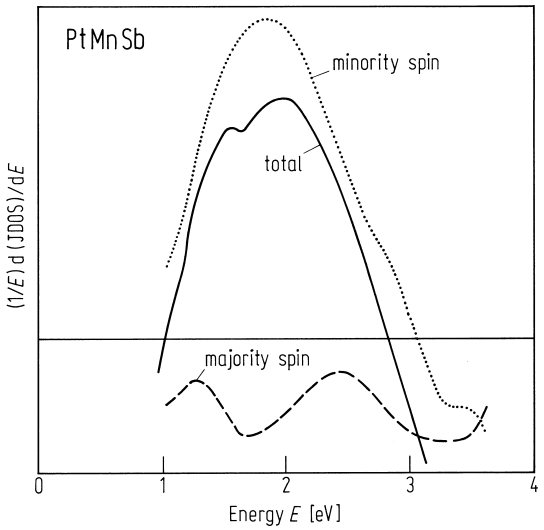

Fig. 629. 1/*E*·d(JDOS)/d*E* vs. *E* of PtMnSb, where *E* is the photon energy $h\nu$ and JDOS is joint density of states calculated by van der Heide et al. Each component of 1/*E*·d(JDOS)/d*E* for majority and minority spin bands is shown by broken and dotted curves, respectively, and the sum is shown by a solid curve [91T1].

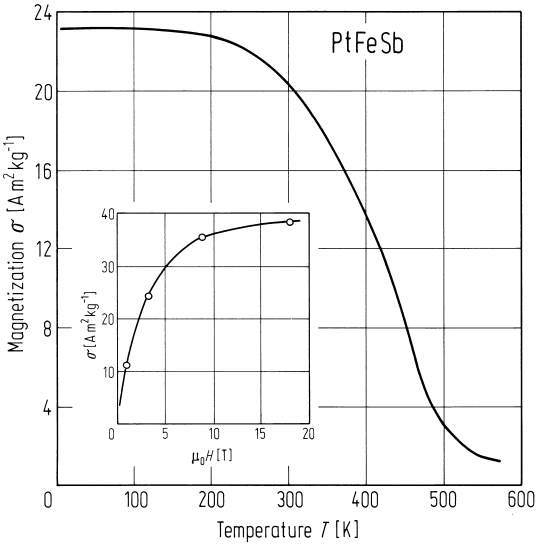

Fig. 630. Temperature dependence of the magnetisation of PtFeSb measured in 0.3 T. The inset shows the field dependence of the magnetisation at 4.2 K [83B3].

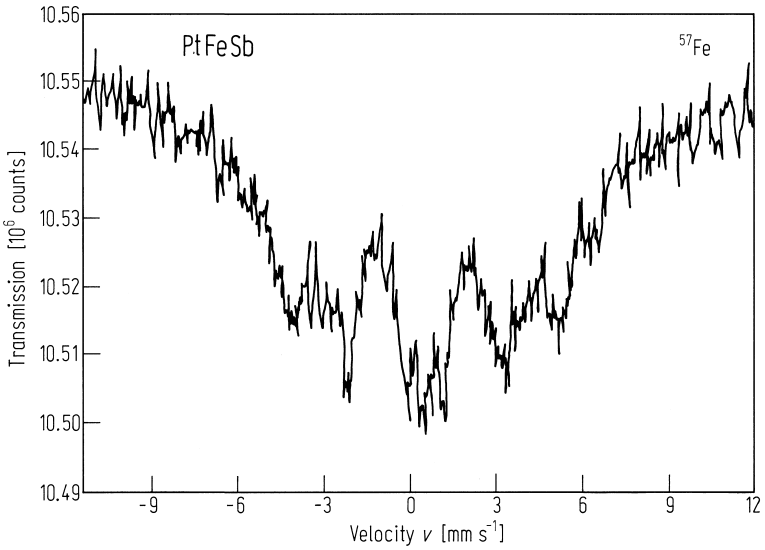

Fig. 631. ^{57}Fe Mössbauer spectrum at 300 K of the compound PtFeSb [83B3].

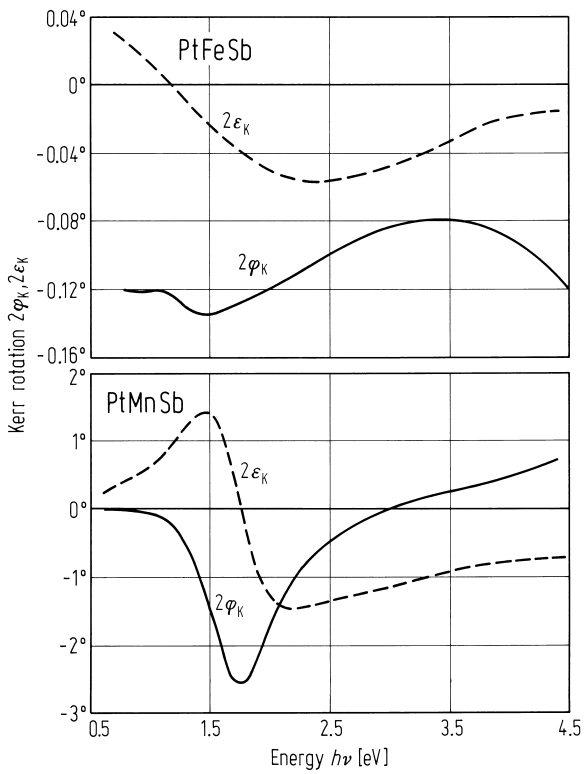

Fig. 632. Double Kerr rotation angle $2\varphi_K$ at room temperature as a function of energy in PtFeSb (top) and PtMnSb (bottom). The broken curve represents the Kerr ellipticity $2\varepsilon_K$ [83B3].

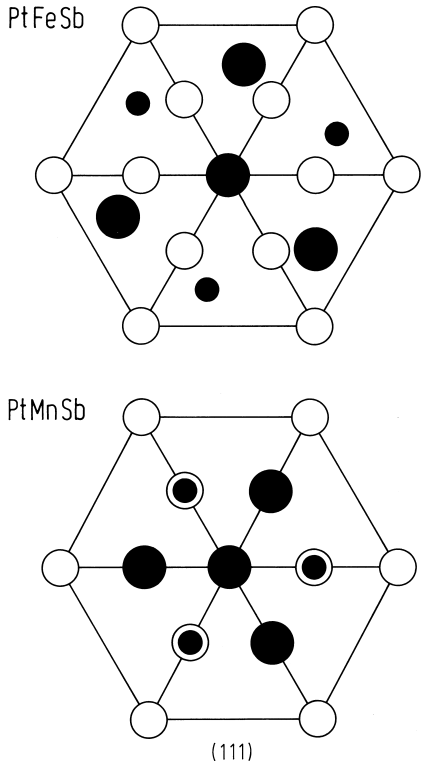

Fig. 633. Projection of the atomic arrangement in PtFeSb and PtMnSb on the (111) planes [83B3].

Films

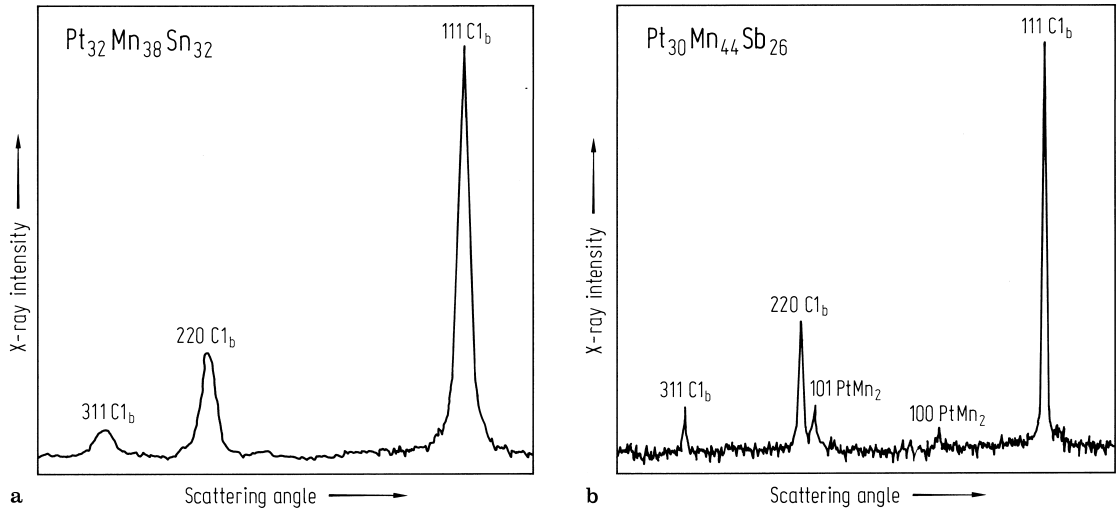

Fig. 634. X-ray diffractometer traces from **(a)** $Pt_{32}Mn_{38}Sn_{32}$ and **(b)** $Pt_{30}Mn_{44}Sb_{26}$ films 300 nm thick and annealed at 500 °C [89A1].

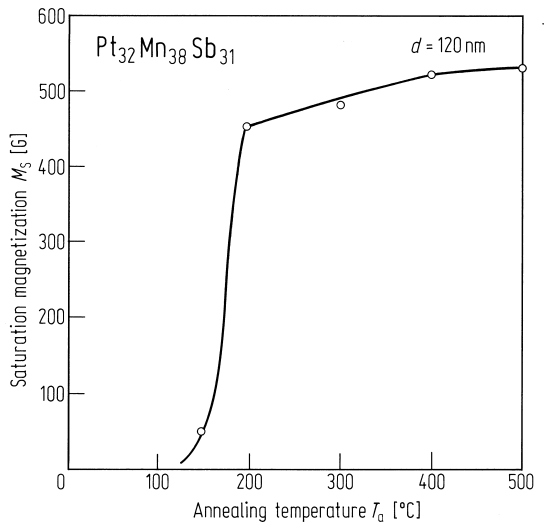

Fig. 635. The saturation magnetisation M_s as a function of annealing temperature for an 120 nm $Pt_{32}Mn_{38}Sb_{31}$ film [89A1].

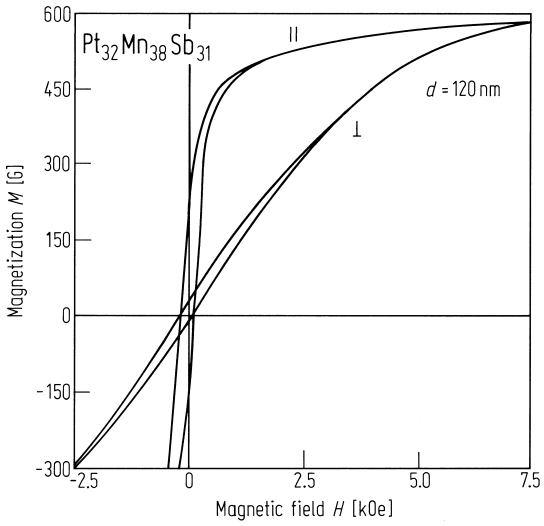

Fig. 636. Perpendicular and in plane hysteresis loops for an 120 nm $Pt_{32}Mn_{38}Sb_{31}$ film annealed at 500 °C [89A1].

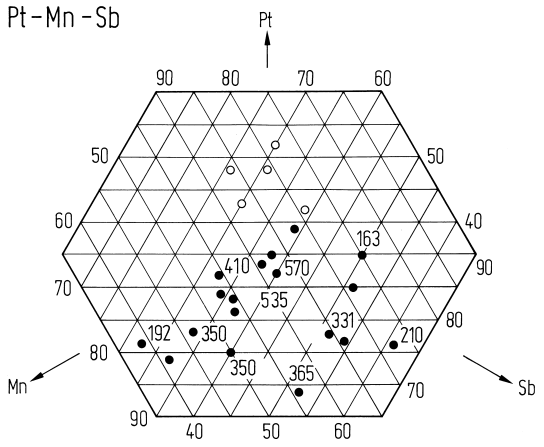

Fig. 637. Magnetic phase diagram of Pt-Mn-Sb films. Composition in at%. Solid circles: ferromagnetic, numbers providing the saturation magnetization M_s in G; open circles: non magnetic [89A1].

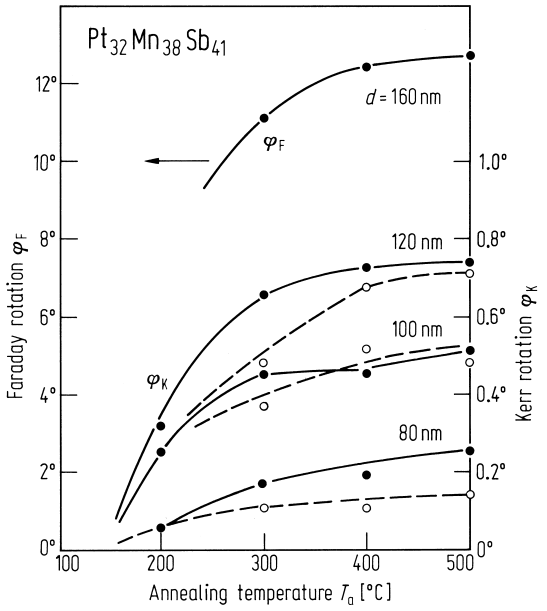

Fig. 638. The Faraday φ_F and polar Kerr φ_K rotations for $Pt_{32}Mn_{38}Sb_{41}$ films of different thickness as a function of annealing temperature.
d = 160 nm, 120 nm, 100 nm and 80 nm [89A1].

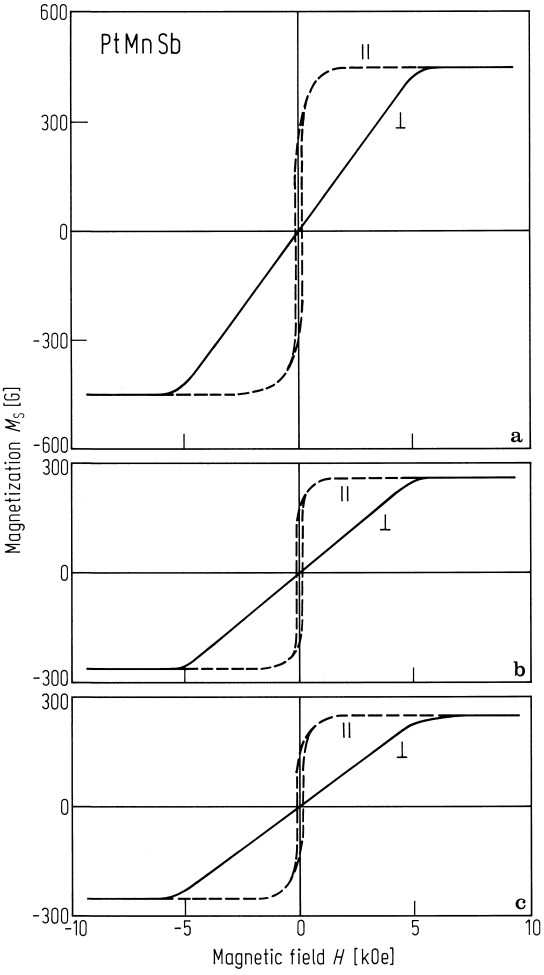

Fig. 640. Magnetisation of PtMnSb films [87I3].

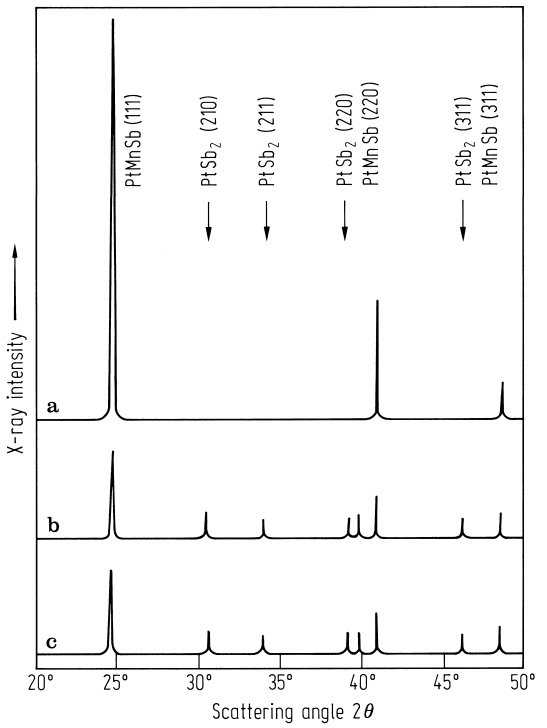

Fig. 639. X-ray diffraction patterns of PtMnSb films: (**a**) $C1_b$ phase; (**b**) C2 phase; (**c**) differs from (**b**) only by a longer annealing time [87I3].

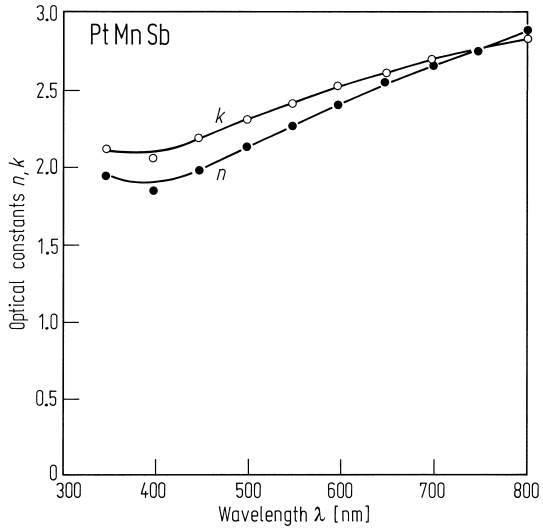

Fig. 641. Optical constants of an as deposited PtMnSb film [92B1].

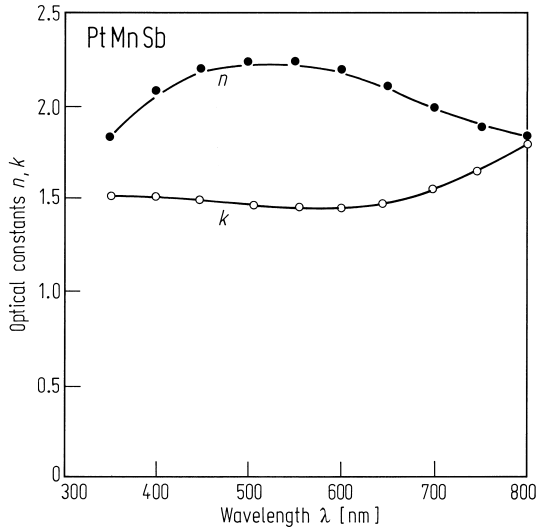

Fig. 642. Optical constants of an annealed PtMnSb film [92B1].

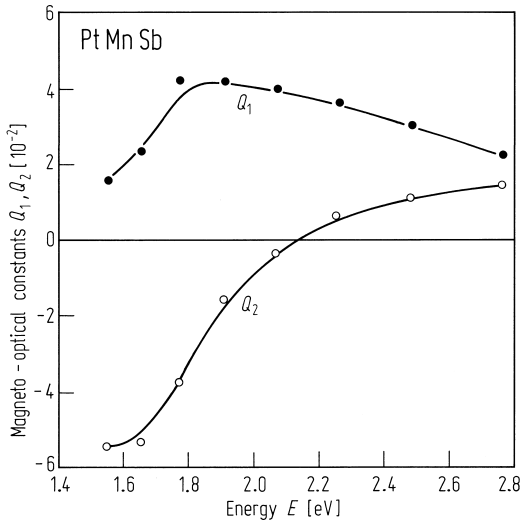

Fig. 643. Magneto-optical constants of an annealed PtMnSb film [92B1].

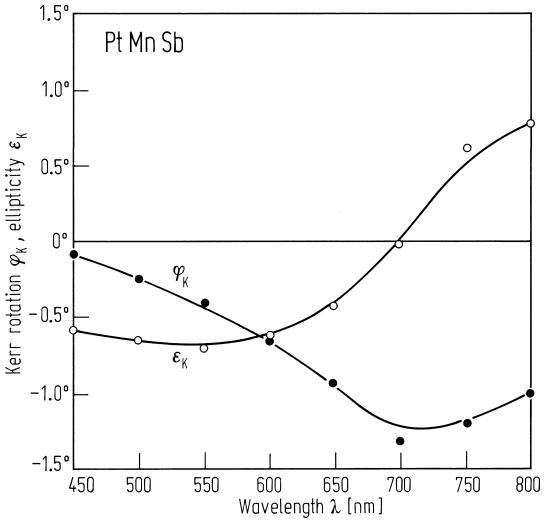

Fig. 644. Calculated polar Kerr effect for a PtMnSb film [92B1].

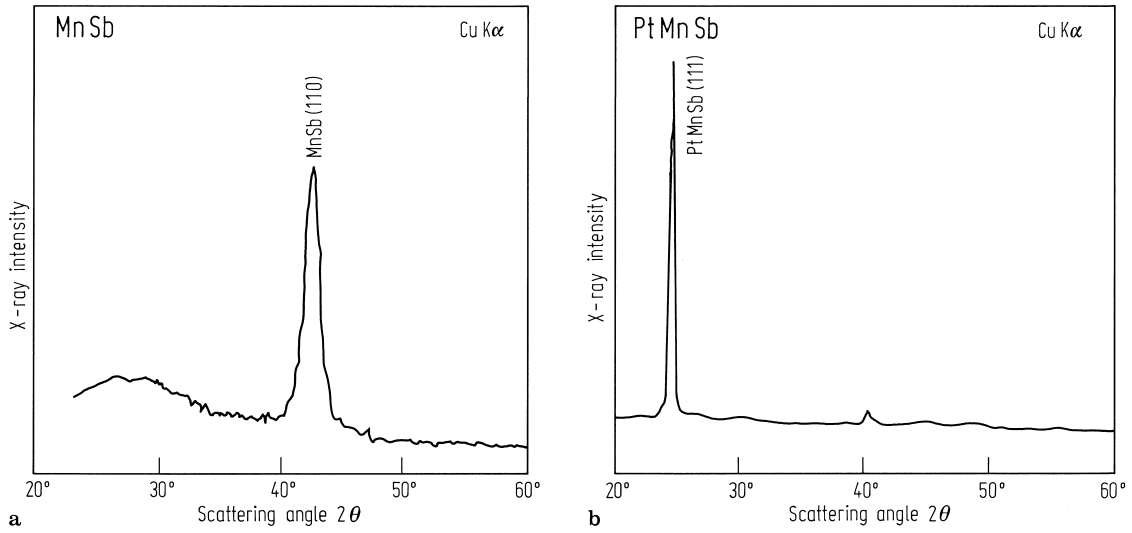

Fig. 645. X-ray diffraction patterns from sputtered (**a**) MnSb and (**b**) PtMnSb alloy films [87S3].

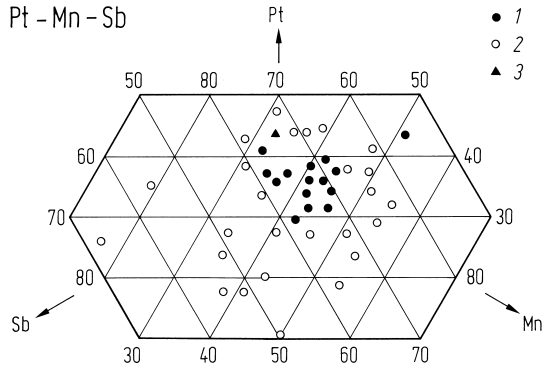

Fig. 646. Relationship between Kerr rotation and composition (in at%) for sputtered PtMnSb alloy films deposited at room temperature. *1*: polycrystalline samples showing Kerr effect, *2*: amorphous samples without Kerr effect, *3*: theoretical composition [87S3].

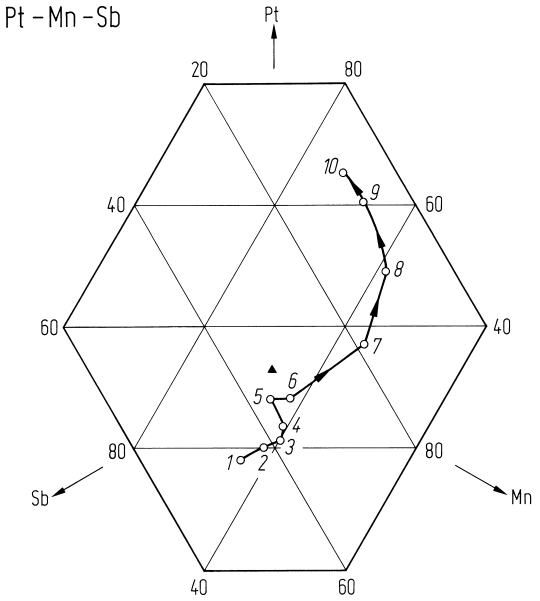

Fig. 647. Kerr rotation and composition (in at%) of PtMnSb films sputtered with dc bias applied (H_{ex} = 7 kOe). Solid triangle: theoretical composition of PtMnSb Heusler alloy [87S3].

Sample	Bias [V]	θ_K
1	0	0.19
2	–10	0.25
3	–20	0.29
4	–30	0.47
5	–40	0.52
6	–45	0.48
7	–50	0.07
8	–60	0
9	–80	0
10	–100	0

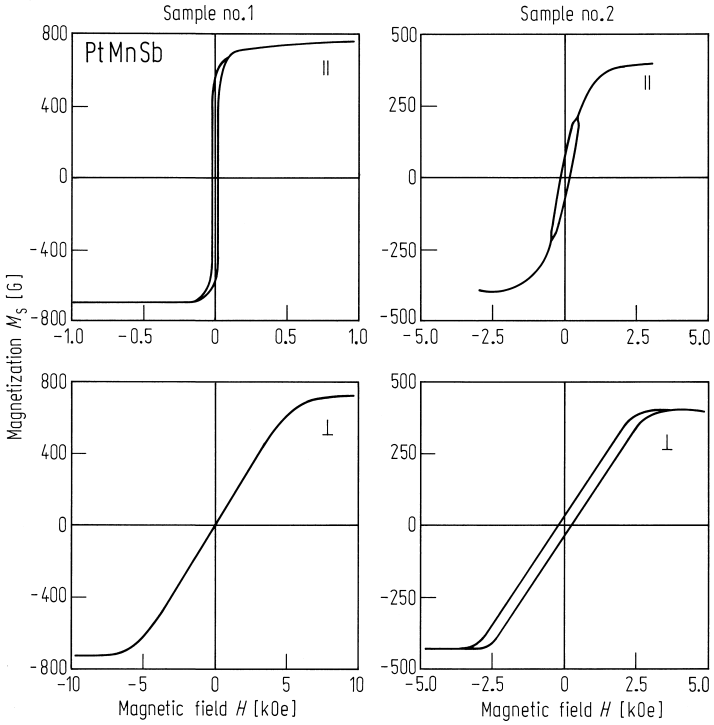

Fig. 648. Hysteresis loops for samples nos. 1 and 2 of PtMnSb alloy films sputtered onto heated glass substrates with T = 200 °C and 400 °C, respectively [87S3].

Table 131. Kerr angles of PtMnSb films deposited onto glass substrates at 200 °C and 400 °C for H_{ex} = 0.75 T [87S3].

Sample	T_{sub} [°C]	$2\varphi_K$
1	200	0.83° (film side)
2	400	1.18° (glass side)

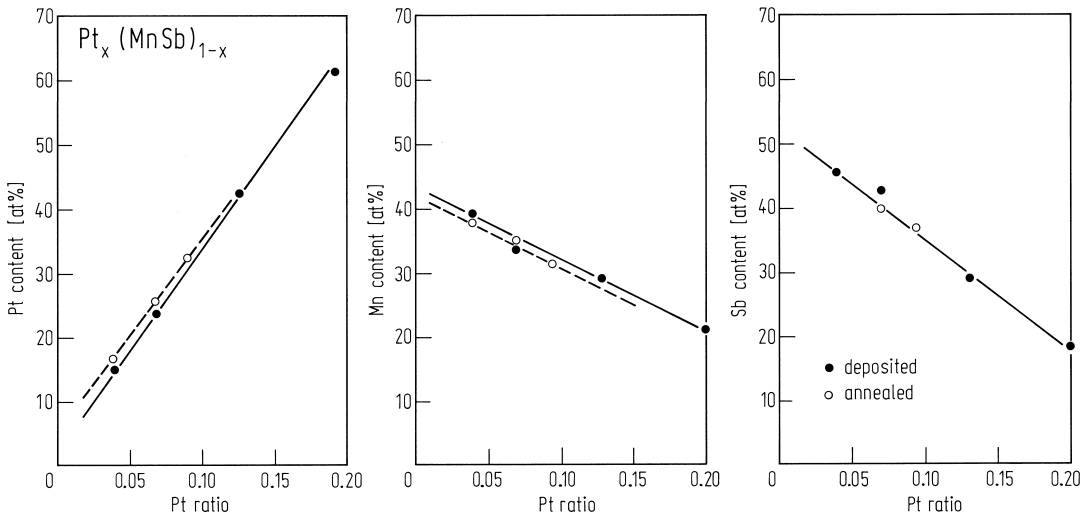

Fig. 649. Pt, Mn and Sb concentrations in as-deposited and annealed $Pt_x(MnSb)_{1-x}$ ($0 \le x \le 0.42$) films vs. Pt area ratio on the composite target [87O1].